SUPPORTING INFORMATION

Easy Accommodation of Different Oxidation States in Iridium Oxide Nanoparticles With Different Hydration Degree as Water Oxidation Electrocatalysts

Alessandro Minguzzi[*a,b], Cristina Locatelli[a,b], Ottavio Lugaresi[a], Elisabetta Achilli[b], Giuseppe Cappelletti[a], Marco Scavini[a,b,d], Mauro Coduri[a,e], Paolo Masala[a], Benedetta Sacchi[a], Alberto Vertova[a,b,d], Paolo Ghigna[c], Sandra Rondinini[a,b,d]

[a]Dipartimento di Chimica, Università di Milano, Via C. Golgi 19, I-20133 Milano, Italy

[b]Consorzio Interuniversitario Nazionale per la Scienza e Tecnologia dei Materiali – INSTM, Milano Unit; Via Golgi 19, 20133 Milano, Italy

[c]Department of Chemistry, University of Pavia, via Taramelli 18, Pavia, Italy

[d]CNR, Istituto di Scienze e Tecnologie Molecolari - ISTM, Via Golgi 19, 20133 Milano, Italy

[e] CNR, Istituto per l'Energia e le Interfasi, - IENI, C.so Promessi Sposi 29, 23900 Lecco, Italy

*Corresponding Author: alessandro.minguzzi@unimi.it

Contents

1. Rietveld Refinement and Williamson-Hall analysis on XRPD patterns of samples P1 and P2

Table S1. Rietveld Refinement and Williamson-Hall analysis on XRPD patterns of samples P1 and P2

	Sample	P1	P2
NaCl	Space group	*Fm*-3*m*	*Fm*-3*m*
	a/Å	5.6450(3)	5.6437(5)
	WF/%	23.1(3)	6.4(1)
Ir	Space group	*Fm*-3*m*	*Fm*-3*m*
	a/Å	3.8365(3)	3.8406(1)
	D_V/Å	26.5(7)	70 (1)
	ε(Δa/a)	0.0087(7)	0.0014(2)
	WF	76.9(1)	33.2(1)
IrO_2	Space group		$P4_2/mnm$
	a/Å	-----	4.5031(8)
	c/Å	-----	3.1446(6)
	D_V/Å	-----	37(1)
	ε(Δa/a)	-----	0.0057(5)
	WF/%	----	60.4(2)
	U_{mean}/ Å^2	0.00065(17)	0.00040(11)
	$R(F^2)$	0.0167	0.0179
	R_P	0.0228	0.0302

2. Williamson Hall plots for metallic Ir phases in P1, P2 samples and for IrO_2 phase in P2 sample.

Figure S1 (left) reports on the WH plots of metallic Ir phases in P1 (black circles) and P2 (red circles) samples as well as for IrO_2 phase (blue squares) in P2 sample.

As to the Ir phase in P1 sample, a noticeable dispersion of the βcosθ values is apparent in the plot in respect to the expected linear dependence *vs.* $\sin\theta$ (see figure **S1** left). However, the dispersion should not be related to bad data quality at least at low angles where peaks are less superimposed. As an example figure S1 right, shows the fits of peaks (111) and (200) after subtraction of background and NaCl peaks, for sake of clarity. A possible source of dispersion of βcosθ values could be related e.g. to the shape of the nanocrystals: as an example (hhh) peaks are sharper than (h00) ones suggesting that Ir grows up preferentially perpendicularly to the close packed layers. However it is not possible to recognize a well-defined (hkl) dependence of peaks integral breadth.

The data dispersion is much smaller for the same phase in P2 sample.

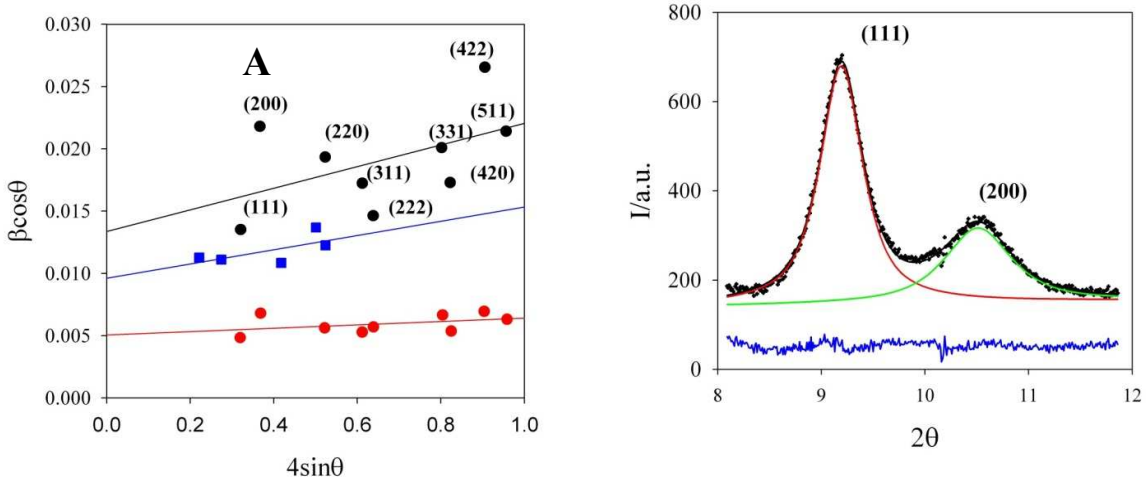

Figure S1. Left: Williamson Hall plots for metallic Ir phases in P1 (black circles) and P2 (red circles) samples and for IrO2 phase (blue squares) in P2 sample. Right: Fit of (111) and (200) reflections of Ir phase in P1 sample using pseudo-Voigt functions. Measured (black crosses) and calculated (red line) profiles are shown as well as residuals (blue line)

3. Real space Rietveld analysis of the PDF data pertinent to P1 and P2 samples.

In this section the PDF analysis of XRPD patterns collected on samples P1 and P2 at the ID15 beamline of the ESRF is reported. Figure S2 displays the experimental G(*r*) function for both samples in a wide *r* range. A damping of the G(*r*) peaks with increasing *r* is apparent, more marked for the P1 sample then for P2. This is consistent with the nanostructured nature of both samples as demonstrated by the WH analysis. It should be noted that also the low Q resolution of the ID15 beamline contributes to this phenomenon.

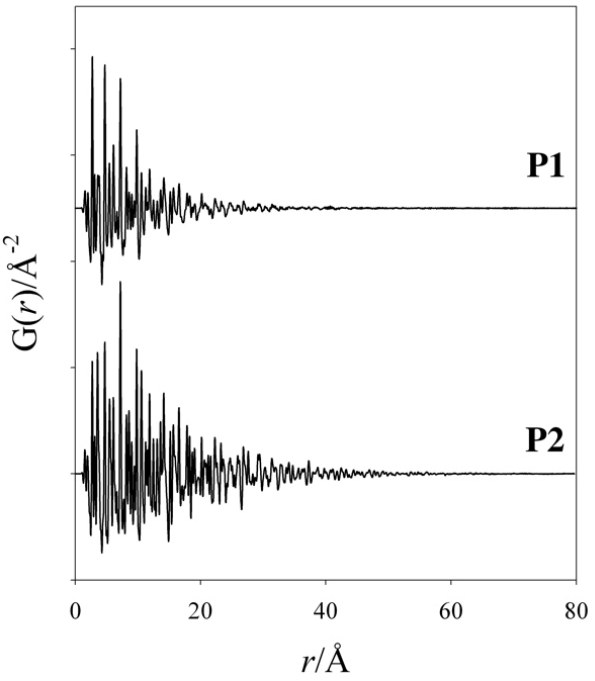

Figure S2. Experimental G(*r*) curves for P1 (up) and P2 (down) samples

Starting the data analysis from the P1 sample, in Figure **S3** the experimental G(*r*) function is fitted against the structural model obtained by Rietveld analysis (hereafter model "0"). To take into account the nanostructured nature of the Ir phase, a curve envelope parameter has been introduced fitting the data in the 1.5-60 Å range. Then, the fit has been applied to the low *r* data (r<10 Å) taking fixed the envelope parameter and varying cell constants, weight fractions and an average mains square parameter (see Table S2). A poor fit is obtained (R=0.39) and huge differences between experimental and calculate curves are apparent for r<5 Å where several experimental G(r) peaks are not considered in the fit at $r \approx 2.0$, 3.1 and 3.6 Å (see Figure S3, left). Conversely, at wider *r* ranges a

better fit is obtained and all the experimental peaks are considered in the structural model (see e.g. the 5<*r*<20 Å range as reported in Figure S3, right**.**

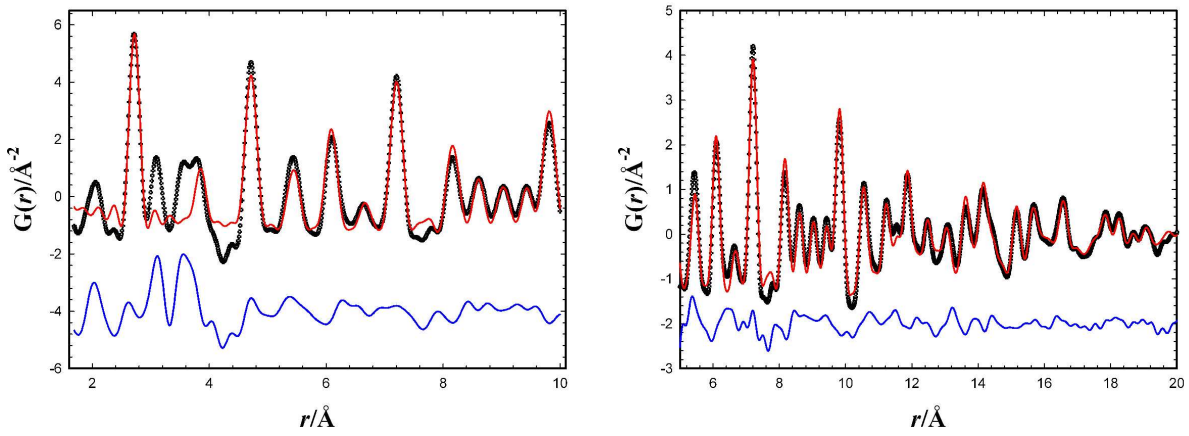

Figure S3. Experimental (black crosses) and calculated (red line) G(*r*) functions, as well as residuals (blue line) for P1 sample applying "Model "0" at different *r* ranges

As shown in Figure 3 of the main text, the G(*r*) peaks not considered by the fit correspond to Ir-O and Ir-Ir distances of IrO_2 compound. For this reason a rutile like IrO_2 phase has been introduced in the structural model (see Figure S4, left). Besides all the parameters listed above, also the IrO_2 cell parameters, weight fraction and an envelope parameter have been added to the fit (see "model 1" in Table S2). The ratio between NaCl and Ir phases is quite similar to the Rietveld analysis; moreover Ir crystallite diameter D as determined by G(*r*) (D≈30 Å) is close to the WH value (D_V=27 Å). According to PDF, the most abundant phase in the sample is IrO_2 (WF≈0.73), whose diffraction peaks were not observed in the Rietveld analysis. This suggests that IrO_2 exists as an amorphous phase in P1 sample. As a matter of fact, the envelope parameter (D≈7 Å) has not to be considered the crystallite dimension but an indication of the extension of short range order in IrO_2 phase.

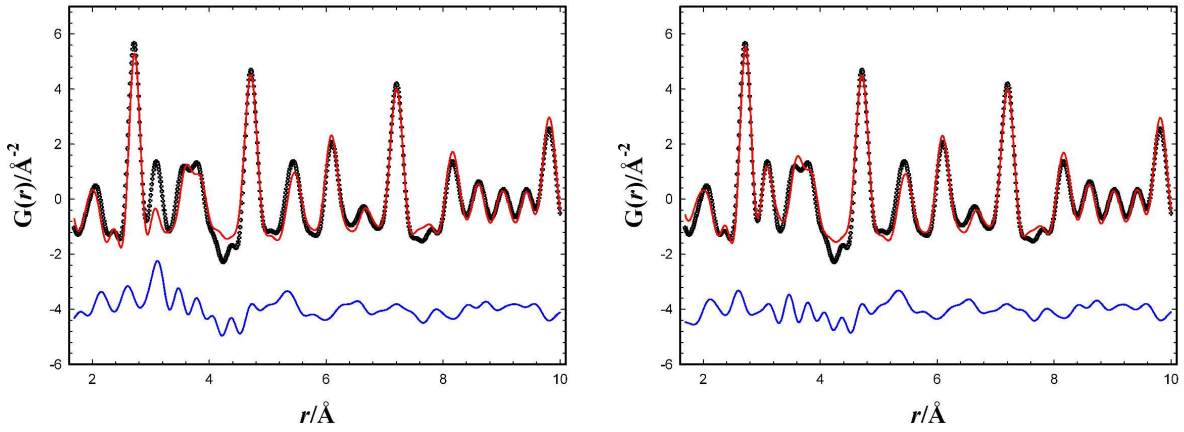

Figure S4. Experimental (black crosses) and calculated (red line) G(*r*) functions, as well as residuals (blue line) for P1 sample applying "Model 1" (left) and "Model 2" (right)

Despite the improvement of the fit quality in respect to "model 0" some discrepancies are still present. In particular the peak at $r \approx 3.1$ Å, which matches up with Ir-Ir distance along the c axis is underestimated. As a matter of fact, the rutile structure is build up by Ir-O octhahedra which are jointed together by an edge along the *c* axis and by corners along the <110> direction. We may suppose that order is more extended along the c axis than in the ab plane, due to the rigidity of Ir octhahedra in that direction. Since the envelope parameter implies an isotropic decrease of the G(*r*) peaks amplitude with increasing *r*, this brings to underestimate the intensity of peak at 3.1 Å.

To map the *directional order* along the *c* axis, we described the IrO_2 phase using both the rutile structural model and a supercell (4a×4a×4c wide) containing only two Ir-O octhahedra connected by a corner perpendicular to the c axis with the Ir-Ir distance along the c axis (hereafter "model 2"). In the new fit the values of cell constants, thermal parameters and envelope parameters for the two IrO_2 phases have been kept equal. The result of the new fit is shown in Figure S4, right, while the fitted data are reported in Table S2. The improvement of the fit quality suggests that in IrO_2 phase partial order along the *c* axis is preserved at least at the local scale. However, due to the multiphase nature of the sample and to the superimposition of most of the G(*r*) peaks, "model 2" has to be considered as qualitative, and refined parameters have scarce significance. We report them in Table S2 for sake of completeness.

As to the P2 sample, we adopted the same structural models as for P1. In particular the experimental and calculated G(*r*) curves at low *r* values applying "model 1" are shown in the left hand side of Figure S2, while the fitted parameters are reported in Table S2. When G(*r*) is investigated at large *r* values (up to 60 Å) the fitted WF for IrO_2 phases is ≈0.60 (not shown), in accord with the reciprocal

space analysis (see Table S1). Conversely, the low *r* fit indicate WF(IrO_2) ≈0.76, as for P1 sample (see Table S2). A possible explanation of this discrepancy is that even in P2 sample IrO_2 phase is partially amorphous or at least very disordered. Accordingly, also for P2 sample, the G(*r*) peak at $r \approx$ 3.1 Å is underestimated.

When the *qualitative* "model 2" is applied to sample P2, the fit quality is improved not only around $r \approx$ 3.1 Å but also nearby $r \approx 6.2$ Å that is the 2nd Ir-Ir distance along the c axis. (see Figure S5, right). Also in this case we must warn about the scarce significance of the fitted parameters.

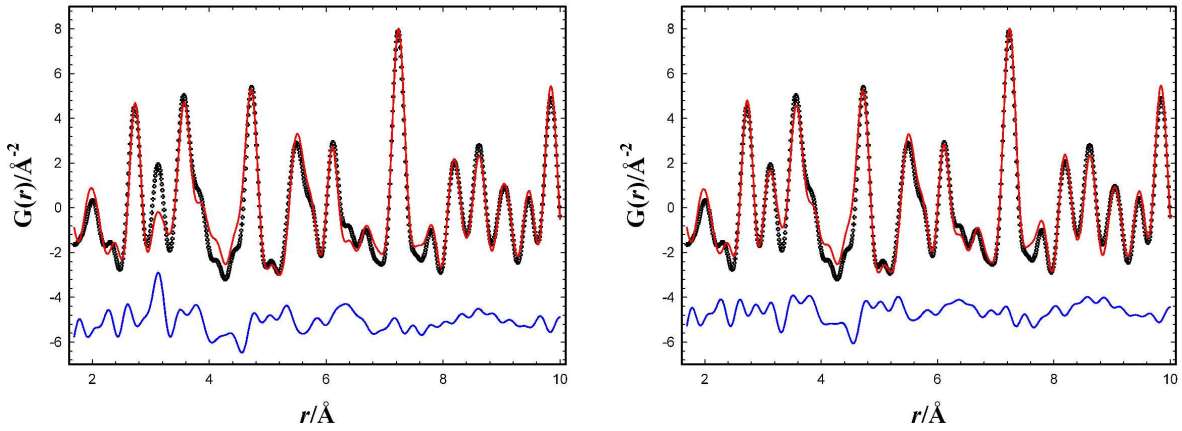

Figure S5. Experimental (black crosses) and calculated (red line) G(*r*) functions, as well as residuals (blue line) for P2 sample applying "Model 1" (left) and "Model 2" (right)

Table S2. Real space Rietveld refinement of the G(*r*) curves in the $1.6 \leq r \leq 10$ Å range applying different structural models ESDs are in brackets.

	Sample	IrO2_NP			IrO2_Wet	
	model	Mod_0	Mod_1	Mod_2	Mod_1	Mod_2
NaCl	Space gr.	*Fm*-3*m*	*Fm*-3*m*	*Fm*-3*m*	*Fm*-3*m*	*Fm*-3*m*
	a/Å	5.33(7)	5.598(4)	5.614(3)	5.566(1)	5.566
	U/ Å^2	≡ Ir	≡ Ir	≡ Ir	≡ Ir	≡ Ir
	WF/%	0.014(3)	0.06(2)	0.034(1)	0.08(2)	0.04(1)
	delta_2	----	----	----	----	----
Ir	Space gr.	*Fm*-3*m*	*Fm*-3*m*	*Fm*-3*m*	*Fm*-3*m*	*Fm*-3*m*
	a/Å	3.8349(1)	3.8346(1)	3.8345(1)	3.84495(5)	3.84450 (4)
	D_V/Å	30.4	30.4	30.4	87.2	87.2
	U/ Å^2	0.00515(3)	0.00564(3)	0.00593(3)	0.00346(1)	0.00360(1)
	WF%	0.986(3)	0.206(2)	0.093(1)	0.163(1)	0.105(1)
	delta_2	3.92(9)	3.96(8)	3.93(7)	2	2
IrO_2	Space gr.	--------	$P4_2/mnm$	$P4_2/mnm$	$P4_2/mnm$	$P4_2/mnm$
	a/Å	--------	4.619(2)	4.602(2)	4.5269(3)	4.5290(2)
	c/Å	--------	3.095(3)	3.098(1)	3.1420 (4)	3.1252(3)
	U/ Å^2	--------	0.0070(2)	0.0091 (1)	0.00623(2)	0.00666 (2)
	D_V/Å	--------	6.84(4)	6.45(4)	13.9 (3)	14.02(3)
	WF/%	--------	0.734(3)	0.873(9)	0.757(1)	0.855(2)
	delta_2	--------	1.5(1)	1.5	1.5	1.5
	R_P	0.393	0.282	0.198	0.241	0.202

4. Interatomic distances for the first and the second coordination shells of oxygen atoms for el_1 and el_2 and their Debye Waller Factors for el_1 and el_2.

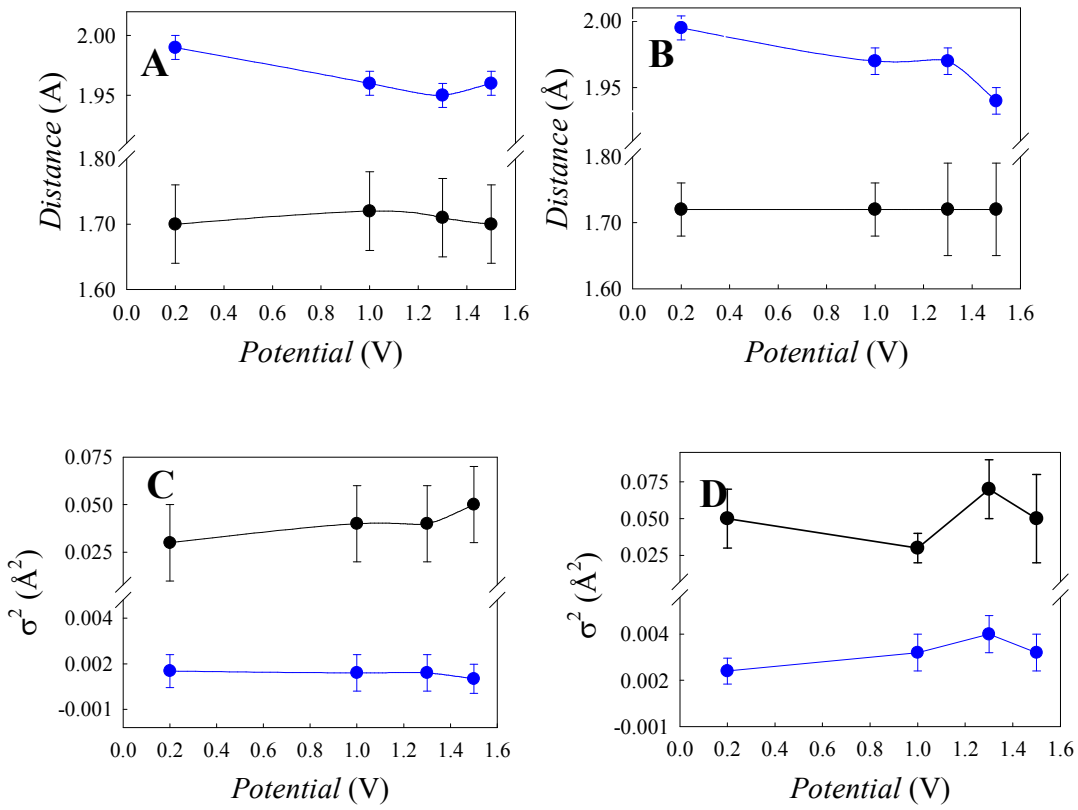

Figure S6: Interatomic distances for the first and the second coordination shells of oxygen atoms for el_1 (A) and el_2 (B) and their Debye Waller Factors for el_1 (C) and el_2 (D). The model employed for the EXAFS fitting procedure is characterized by 6 oxygen atoms arranged in a distorted octahedral: the two apical are situated at a shorter distance.

5. Calculation and subtraction of Metallic Ir contribution in XANES spectra and fitting for applied potentials < 1.0 V and > 1.0 V.

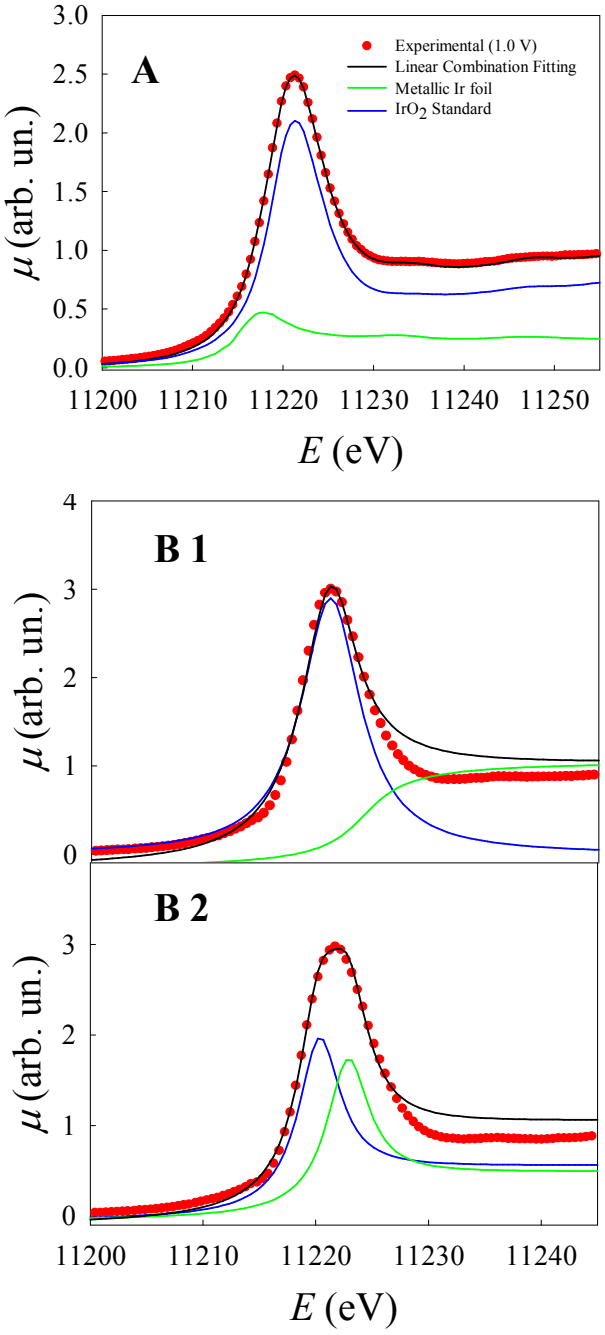

Figure S7: A) Fitting of XANES spectrum recorded at 1.0 V by means of a linear combination of Metallic Ir Standard (25 %) and IrO_2 standard (75%) spectra. B) Fitting of XANES spectra after the subtraction of metallic iridium contribution for applied potential < 1.0 V (1) and for applied potential > 1.0 V (2). In the first case the fitting was carried with a linear combination of an arc tangent and a lorentzian function, in the latter with an arc tangent and two lorentzian functions.